Measurement report: The effect of aerosol chemical composition on light scattering due to the hygroscopic swelling effect

Rongmin Ren[1], Zhanqing Li[2], Peng Yan[3], Yuying Wang[4], Hao Wu[5], Wei Wang[1], Xiao'ai Jin[1], Yanan Li[3],
Dongmei Zhang[1] and Maureen Cribb[2]

[1]State Key Laboratory of Remote Sensing Science, College of Global Change and Earth System Science, Beijing Normal University, Beijing 100875, China
[2]Earth System Science Interdisciplinary Center, Department of Atmospheric and Oceanic Science, University of Maryland, College Park, College Park, MD, USA
[3]CMA Meteorological Observation Center, Centre for Atmosphere Watch and Services, Beijing 100081, China
[4]Key Laboratory for Aerosol-Cloud-Precipitation of China Meteorological Administration, School of Atmospheric Physics, Nanjing University of Information Science and Technology, Nanjing 210044, China
[5]School of Electrical Engineering, Chengdu University of Information Technology, Chengdu 610225, China

Correspondence to: Zhanqing Li (zli@atmos.umd.edu)

Abstract. Liquid water in aerosol particles has a significant effect on optical properties, especially on light scattering, whose dependence on chemical composition is investigated here using measurements made in southern Beijing in 2019. The effect is measured by the enhancement of aerosol hygroscopic factor, $f(\text{RH} = 85\%, 525 \text{ nm})$, which is found to be positively and negatively impacted by the proportions of inorganic and organic matters respectively. Black carbon is also negatively correlated. The positive impact is more robust when the inorganic matter mass fraction was smaller than 40% (correlation coefficient, R = 0.93) which becomes weaker as the inorganic matter mass fraction gets larger (R = 0.48). A similar pattern was also found in the negative impact for organic matter mass fraction. Nitrate played a more significant role in aerosol hygroscopicity than sulfate in Beijing. However, the deliquescence point of ambient aerosols was at about RH = 80% when the ratio of the sulfate mass concentration to the nitrate mass concentration of the aerosol was high (mostly higher than ~4). Two schemes to parameterize $f(\text{RH})$ were developed in accounting for the deliquescent and non-deliquescent effects. Using only one $f(\text{RH})$ parameterization scheme to fit all $f(\text{RH})$ processes would incur large errors. A piecewise parameterization scheme is proposed, which can better describe deliquescence and reduces uncertainties in simulating aerosol hygroscopicity.

1 Introduction

Atmospheric aerosols have impacts on visibility, the earth-atmosphere radiation budget, cloud and precipitation via direct and indirect effects (IPCC, 2013). Both effects are associated with the hygroscopic properties of aerosols and relative humidity (RH) of the atmosphere. The hygroscopic enhancement factor ($f(\text{RH}, \lambda)$) is the ratio of the scattering coefficient at an ambient RH level to that under a fixed low RH level (RH < 40%) at a certain light wavelength (λ). It has been characterized during field experiments taking place around the world (Fierz-Schmidhauser et al., 2010a, b; Zieger et al., 2010, 2014), and in China

Atmospheric
Chemistry
and Physics
Discussions

(Yan et al., 2009; Zhang et al., 2015; Kuang et al., 2016; L. Liu et al., 2018; C. Zhao et al., 2019; P. Zhao, 2019; T. Wu et al.,

35   2020).

Aerosol chemical composition has a strong impact on aerosol hygroscopicity (Fierz-Schmidhauser et al., 2010a, b; Y. Wang et al., 2017, 2018, 2019). Zhang et al. (2015) studied the relationship between the scattering enhancement factor and chemical composition in Lin'an, China, and found that nitrate had a stronger effect on aerosol hygroscopicity than sulfate partially due to the rigid control of SO_2 that reduce the amount of sulfate. Zieger et al. (2014) analyzed the correlation between the chemical

40   composition of aerosols and f(RH = 85%, 550 nm) in Melpitz, Germany, and noted negative and positive impacts by organic and black carbon (BC) and by inorganic substances, such as ammonium, respectively. However, the correlation between the mass fractions of individual (NO_3^-) and (SO_4^{2-}) and f(RH = 85%, 550 nm) were weak. Unlike previous studies, Jin et al. (2020) reported that apart from inorganic matter, e.g., (SO_4^{2-}) and (NO_3^-), organic species also significantly contributed to the aerosol liquid water content. They proposed that in the initial phase of a pollution event, the aerosol liquid water content contributed

45   by organic matter accelerated aqueous-phase reactions, converting gaseous precursors into secondary aerosols, which then absorb more liquid water.

Air pollution has been a severe problem in China, especially in megacities such as Beijing. A high hygroscopic enhancement factor is one of the most important factors causing degradation in visibility. Some observational studies of the light hygroscopicity enhancement factor in Beijing have been conducted (X. Liu et al., 2013; Yang et al., 2015; G. Zhao et al., 2018;

50   P. Zhao et al., 2019). However, studies exploring the relationship between aerosol chemical composition and the hygroscopic enhancement factor are lacking. Moreover, although several optimal expressions of $f(RH, \lambda)$ for different seasons have been developed (Kuang et al., 2016; Pan et al., 2009; Y. Wu et al., 2017; Yan et al., 2009; Yu et al., 2018; P. Zhao et al., 2019), parameterization of the deliquescent curve of (SO_4^{2-}) in ambient aerosols has not yet been done for the Beijing-Tianjin-Hebei (BTH) metropolitan region, where aerosol deliquescent phenomena frequently occur (Kuang et al., 2016). It is thus important

55   to develop an optimal parameterization to describe this deliquescent phenomenon to improve model simulations of aerosol hygroscopicity.

In this study, $f(RH, \lambda)$ at three wavelengths for RH ranging from 40% to about 90% were measured by a high-resolution humidified nephelometer system deployed in the southern suburban area of Beijing, China. Other aerosol chemical and physical properties were also simultaneously measured. Humidograms were classified into two categories, i.e., deliquescent

60   and non-deliquescent, each parameterized separately. The parameterization results of deliquescent processes agreed well with observations. This result is useful for improving simulations of $f(RH,\lambda)$ of ambient aerosols during deliquescence in the BTH metropolitan region.

The paper is organized as follows. Section 2 describes the instruments and methods. Section 3 presents and discusses the results of this study, and Section 4 provides a summary.

Atmospheric
Chemistry
and Physics
Discussions

2 Instruments and methods

2.1 Observation site

A comprehensive field experiment was conducted at the climate observatory of the China Meteorological Administration, located in Yizhuang, Beijing, near the southern Fifth Ring Beltway (39.81ºN, 116.48ºE) surrounded primarily by residential communities, and industrial parks (Fig. 1). The measurements can characterize the aerosol chemical and physical properties of a typical suburban area of this megacity in the North China Plain. Equipped with a multitude of instruments measuring, for example, optical, hygroscopic, and chemical properties of aerosols (Li et al., 2019), this study employs only those measurements acquired from 19 September to 4 October 2019.

2.2 Instruments

A dual-nephelometer system (Aurora 3000, Ecotech) with a high time resolution was used to measure the aerosol hygroscopic enhancement factor. After an aerosol sample passed through the Nafion dryer (MD-700-48F-5, Perma Pure LLC), the dry sample flow (RH < 40%) was divided into two routes. One sample flow went straightly into the dry nephelometer. The other sample flow passed through a humidifying tube to be humidified to a given RH, following the humidifying scheme put forward by Carrico et al. (1998), then channeled into the wet nephelometer. The scattering coefficients under dry (usually < 40%) and wet ambient conditions were measured synchronously by the two nephelometers (Yan et al., 2009). To improve the performance of this system and to decrease the amount of time needed to undergo one aerosol humidifying process, two water baths were used in turn to heat the water circulating in the interior layer of the humidifying tube (Liu and Zhao, 2016).

Full calibrations of the two nephelometers were performed once a month. The calibration tolerance of the zero check was ±2 Mm^{-1}, and that of the span check was ±2% of the span point. Calibrations of the two nephelometers in the dry state were consistent (Fig. S1). Because the RH measured by the probes built into the optical chambers of the nephelometers were imprecise, the method described by Liu and Zhao (2016) and Kuang et al. (2017) was used to correct this. First, two calibrated RH and temperature probes (HMP110, Vaisala; accuracy of ±0.2°C for the 0–40°C temperature range and ±1.5% RH and ±2.5% RH for the 0–90% and 90–100% RH ranges, respectively) were placed at the inlet and outlet of the wet nephelometer, obtaining 1-min averages of RH and temperature. The RH and temperature measured by the probe at the outlet of the wet nephelometer (RH$_{outlet}$ and T_{outlet}) were then used to calculate the dew-point temperature, $T_{dew-point}$:

$$T_{dew-point} = RH_{outlet}^{\frac{1}{8}}(112 + 0.9T_{outlet}) + 0.1T_{outlet} - 112. \tag{1}$$

Finally, RH in the optical chamber (RH$_{chamber}$) was corrected, based on the temperature in the optical chamber ($T_{chamber}$) and $T_{dew-point}$:

$$RH_{chamber} = (\frac{112 - 0.1T_{chamber} + T_{dew-point}}{112 + 0.9T_{chamber}}). \tag{2}$$

An aerosol chemical speciation monitor (ACSM; Aerodyne Research Inc.) measured the mass concentrations of non-refractory
95   aerosol chemical species, including SO_4^{2-}, NO_3^-, ammonium (NH_4^+), chlorine (Chl), and organics (Org) in particulate matter
with diameters less than 2.5 µm ($PM_{2.5}$). A seven-wavelength aethalometer (AE33, Magee Scientific) measured the mass
concentration of BC. The Chinese Ministry of Ecology and Environment network and the Beijing Municipal Environmental
Monitoring Center (http://106.37.208.233:20035/ and http://www.bjmemc.com.cn/) provided mass concentrations of $PM_{2.5}$
measured at the Yizhuang station, about 3 km southeast of the observatory. The LI-COR eddy covariance system (this system
100   includes WindMaster Pro, LI-7500A, and Smart2-00171, LI-COR) measured various meteorological parameters.

2.3 Methods

The hygroscopic enhancement factor, $f(\text{RH}, \lambda)$, is defined as

$$f(\text{RH}, \lambda) = \frac{\sigma_{sp}(\text{RH}, \lambda)}{\sigma_{sp}(\text{RH}_{dry}, \lambda)}, \tag{3}$$

where $\sigma_{sp}(\text{RH}, \lambda)$ represents the scattering coefficient at an elevated RH (usually RH > 40%), and $\sigma_{sp}(\text{RH}_{dry}, \lambda)$ is the
105   scattering coefficient in the dry state (usually RH < 40%) at wavelength λ. The values of $f(\text{RH}, \lambda)$ are generally greater than
1 and increase with increasing RH. In this study, $f(\text{RH} > 40\%)$ is normalized as

$$f(\text{RH} > 40\%)_{normalized} = \left(\frac{f(\text{RH} > 40\%)}{f(\text{RH} < 40\%)_{averaged}} \right). \tag{4}$$

Here, $f(\text{RH} < 40\%)$ equals 1.

The absorption coefficient of $PM_{2.5}$ at 880 nm is calculated by the BC monitor (Han et al., 2015; Zou et al., 2019). To facilitate
110   comparisons, absorption coefficients at 880 nm are transformed into those at 525 nm by assuming that the absorption
coefficient is inversely proportional to the wavelength (Bond and Bergstrom, 2006; C. Liu et al., 2018). The quantity $\omega_{0(525nm)}$
is the aerosol single-scattering albedo at 525 nm. The dependence of light scattering on wavelength is described by the
Ångström exponent ($\alpha_{(\lambda_1 - \lambda_2)}$), an index describing the particle size:

$$\alpha_{(\lambda_1 - \lambda_2)} = \frac{\log\sigma_{sp}(\lambda_1) - \log\sigma_{sp}(\lambda_2)}{\log\lambda_2 - \log\lambda_1}. \tag{5}$$

115   Here, $\alpha_{(450nm - 635nm)}$ between 450 nm and 525 nm is calculated using Eq. (5).

The parameter γ can replace $f(\text{RH})$ in a wider RH range (Doherty et al., 2005; Quinn et al., 2005; Zhang et al., 2015) and is
calculated as follows:

$$\gamma = \frac{\ln f(\text{RH})}{\ln\left(\frac{100 - \text{RH}_{ref}}{100 - \text{RH}}\right)}. \tag{6}$$

Here, $\text{RH}_{ref} = 40\%$ and RH = 85%.
120   The following parameter (F_{org}) denotes the relative amount of organic and inorganic matter:

$$F_{\text{org}} = \frac{C_c}{C_c + C_i},\tag{7}$$

where C_c is the organic matter mass concentration measured by the ACSM, and C_i represents inorganic ion mass concentrations like SO_4^{2-} and NO_3^- measured by the ACSM.

Deliquescence of ambient aerosols was present throughout the study period. To identify this process and describe its magnitude in the 78–82% RH range, the hysteresis index η is defined as

$$\eta = 1 - \frac{g_{<78\%}}{g_{>82\%}}.\tag{8}$$

The terms $g_{<78\%}$ and $g_{>82\%}$ are the fit parameters of the f(RH) parametrization scheme

$$f(\text{RH}) = (1 - \text{RH})^{-g},\tag{9}$$

at RH < 78% and RH > 82%, respectively. The theoretical range of η is 0 to 1. The $g_{<78\%}$ and $g_{>82\%}$ terms, respectively, represent the magnitudes of the scattering enhancement when RH < 78% and RH > 82%. Because the values of $g_{<78\%}$ and $g_{>82\%}$ are about the same, η is close to 0. This suggests that f(RH) increases slowly and continuously when 78% < RH < 82%, and no deliquescence is found. However, when the value of $g_{>82\%}$ is much higher than $g_{<78\%}$, η approaches 1. This explains why the f(RH) cycle has a jump at 78% < RH < 82%, i.e., very distinct deliquescence occurring in the RH range of 78% to 82%. Here, when η is higher than 0.4, deliquescence occurs.

3 Results and discussion

3.1 Overview

Figure 2 depicts the hourly averaged time series of the light-scattering coefficient ($\sigma_{\text{sp,525nm}}$), the absorption coefficient ($\sigma_{\text{ap,525nm}}$), the single-scattering albedo ($\omega_{0(525nm)}$), the scattering Ångström exponent ($\alpha_{(450nm-635nm)}$), and the hygroscopic enhancement factor at RH = 85% (f(RH = 85%, 525 nm)) at the main observatory, and the mass concentration of $PM_{2.5}$ measured at the Yizhuang station from 19 September to 4 October 2019. During this period, the hourly averaged $\sigma_{\text{sp,525nm}}$ ranged from 20 to 952 Mm^{-1} (Fig. 2a), with a mean ± standard deviation value of 266±179 Mm^{-1} (Table 1). The hourly averaged $\sigma_{\text{ap,525nm}}$ varied from 5 to 134 Mm^{-1} (Fig. 2b), with a mean ± standard deviation value of 51±24 Mm^{-1} (Table 1). Figures 2c and 2f show that $\omega_{0(525nm)}$ increased as the $PM_{2.5}$ concentration increased. The hourly averaged $\omega_{0(525nm)}$ during the observation period ranged from 0.49 to 0.93, with an overall mean ± standard deviation value of 0.80±0.09. The mean ± standard deviation values of $\omega_{0(525nm)}$ during clean ($PM_{2.5} \leqslant 35$ μg m^{-3}), moderately polluted (35 μg m^{-3} < $PM_{2.5} \leqslant 75$ μg m^{-3}), and heavily polluted ($PM_{2.5} > 75$ μg m^{-3}) periods was 0.73±0.08, 0.84±0.04, and 0.89±0.02, respectively (Table 1). The $\omega_{0(525nm)}$ increased as $PM_{2.5}$ pollution increased, indicating that, during the contamination process, the proportion of aerosol components with strong scattering properties increased and the proportion of aerosol components with strong absorbing

properties decreased obviously. Higher values of $\omega_{0(525nm)}$ usually occurred when wind was from the northeast at a speed of

150   1–2 m s^{-1} and when relatively stronger winds were from the southeast (Fig. 3a), which was frequently accompanied by a high

proportion of inorganic matter (Fig. 3e) and low proportions of BC (Fig. 3d) and organic matter (Fig. 3f). Figure 2d shows that

the range of $\alpha_{(450nm-635nm)}$ was narrow at most times during the observation period. Relatively larger particles with lower

values of $\alpha_{(450nm-635nm)}$ generally occurred when weak winds were from the east and southeast (Fig. 3b).

During the observation period, f(RH = 85%, 525 nm) ranged from 1.15 to 1.86, meaning a 1.15-to-1.86-fold increase in the

155   scattering coefficient at RH = 85% compared to dry conditions (Fig. 2e). Daily average values of f(RH = 85%, 525 nm) varied

between 1.32 and 1.74, with low values (< 1.40) on 19 and 24 September and relatively high values (> 1.70) on 22 and 28

September and 2 October. Organic matter mass fractions were larger than 52%, and inorganic matter mass fractions were

generally smaller when f(RH = 85%, 525 nm) was less than 1.40. However, high values of f(RH = 85%, 525 nm) in this study

were often closely correlated with large fractions of water-soluble ions, such as NO_3^- and SO_4^{2-}, in $PM_{2.5}$. Inorganic matter

160   mass fractions were larger than 53%, and organic matter mass fractions were relatively small when the f(RH = 85%, 525 nm)

was greater than 1.70. The campaign mean ± standard deviation values of f(RH = 85%, 525 nm)   were 1.64±0.13 (Table 1).

Figure 3c reveals that strongly hygroscopic aerosols with high values of f(RH = 85%, 525 nm) primarily came from the

southeast sector. The proportion of secondary inorganics with strong hygroscopic abilities in aerosols from this direction was

high, while the proportion of organic matter and BC with weak hygroscopic abilities was low (Figs. 3d-f). In the northeast

165   direction, high values of f(RH = 85%, 525 nm) occurred when the wind speed was lower than 2 m s^{-1}, and the hygroscopic

capacity of aerosols also weakened as the wind speed increased (Fig. 3c). The proportion of secondary inorganics with strong

hygroscopicity decreased with increasing wind speed, while the proportion of substances with weak hygroscopicity, such as

organic matter and BC, increased with the increase in northeasterly wind speed (Figs. 3d, f). Furthermore, aerosols from the

southwest and southern sectors within the wind-speed range of 2 to 4 m s^{-1} have higher hygroscopic enhancement factors (Fig.

170   3c), mainly because of the deliquescence of sulfates in the ambient aerosols. The specific reasons are explained in detail in

Section 3.3. Figure S2 shows that apart from the lower values (10th percentile values in Table S1), a small wavelength

dependence in hygroscopic enhancement factor is found in all other percentiles, with a stronger wavelength dependence for

high values of f(RH = 85%). Zieger et al. (2014) and Zhang et al. (2015) obtained similar results for Melpitz, Germany, and

Linan, China, respectively.

175   Figures 4a-c show the time series of the mass concentrations and mass fractions, respectively, of submicron aerosols, i.e.,

organic matter, nitrate, sulfate, ammonium, and chloride, and BC in $PM_{2.5}$. The pie chart on the right of Figure 4c shows

during the entire observation period, organic matter was the major component of $PM_{2.5}$, accounting for 39%. Nitrate and

sulfate comprised similar fractions of $PM_{2.5}$, i.e., 21% and 19%, respectively. The mass fraction of nitrate was slightly larger

than that of sulfate. Note that BC accounted for 11% of $PM_{2.5}$ during the entire measurement period. Throughout the

180   observation period, two special periods are noteworthy. One is from the afternoon of 21 September to late morning on 22

September (section I in Fig. 4a). First, the concentrations of all chemical components during this period were high. As shown

by pie chart on the left of Figure 4c, the mass fraction of nitrate was the largest, accounting for 33% of the total mass fraction on average and lasted a long time. However, compared with the proportion of inorganic matter (66%), the mass fraction of organic matter was much smaller, accounting for 27% of the total mass fraction. Accordingly, the f(RH = 85%, 525 nm)

185   remained at a high level during this period (Fig. 2e). The other special period is 24 September (section II in Fig. 4a). The mass concentrations of all aerosol species remained low. The middle pie chart of Figure 4c clearly demonstrates that organic matter comprised the main fraction of $PM_{2.5}$, accounting for 55% on average, followed by BC. The fraction of nitrate was especially small during this clean period. The fraction of sulfate, accounting for 16%, was four times that of nitrate, which is an advantage for deliquescence in this period (discussed in more detail in section 3.3). Because f(RH = 85%, 525 nm) was higher than normal

190   at the time of deliquescence, f(RH) was not the lowest during the whole observation period, although the proportion of hydrophobic organic matter and BC in the aerosols during this period was very high. Although the proportions of hydrophobic organic matter and BC in the aerosol were very high over the whole observation period, f(RH = 85%, 525 nm) was not the lowest because the f(RH = 85%, 525 nm) of deliquescence was higher than the normal value. Note that $PM_{2.5}$ aerosols at the observatory in suburban Beijing were faintly acidic during the observation period (Fig. S5), benefitting the hygroscopic

195   enhancement of ambient aerosols.

3.2 The relationship between the hygroscopic enhancement factor and aerosol chemical composition

Figure 5 displays f(RH = 85%, 525 nm) as a function of the main chemical component mass fractions. The total aerosol mass concentration is the summary mass concentrations of all chemical constituents, including nitrate, sulfate, ammonium, chloride, and organic matter measured by the ACSM and BC measured by the AE33. The mass fractions of the individual chemical

200   components were calculated by respectively dividing the mass concentrations of sulfate, nitrate, ammonium, and BC by the sum of all chemical constituents. BC and f(RH = 85%, 525 nm) are negatively correlated, with a correlation coefficient R equal to -0.62 in magnitude (Fig. 5d). A positive correlation is seen between f(RH = 85%, 525 nm) and the three other inorganic substances mass fractions because of their hygroscopic characteristics. The ammonium mass fraction has the strongest positive correlation (R = 0.78) with f(RH = 85%, 525 nm) (Fig. 5c). The reason is that ammonium is the common positive ion of

205   ammonium sulfate and ammonium nitrate, two major salts of inorganic substances in aerosols. The relationship between f(RH = 85%, 525 nm) and ammonium is thus similar to that between f(RH = 85%, 525 nm) and inorganic content. The hygroscopic properties are different for ammonium nitrate and ammonium sulfate. As expected, f(RH = 85%, 525nm) was positively correlated with the sum of the nitrate and sulfate mass fractions (slope=1.03 and R=0.79, Fig. S6), similar to the correlation between f(RH = 85%, 525 nm) and inorganic mass fraction. Y. Wu et al. (2017) and Zieger et al. (2014) reported similar results.

210   Figure 6 shows f(RH = 85%, 525 nm) as a function of the mass fractions of organic and inorganic matter. The mass fractions of inorganic and organic matter were respectively calculated by dividing inorganic matter (the sum of nitrate, sulfate, ammonium, and chloride) and organic matter mass concentrations by the total mass concentration. The inorganic mass fraction was positively correlated with f(RH = 85%, 525 nm) because of the high hygroscopicity of the inorganic compounds, while organic substances were negatively correlated with f(RH = 85%, 525 nm) because of their lower hygroscopicity (Zhao et al.,

215   2019). Both correlation coefficients were similar to those from previous studies (Zeiger et al., 2014; Zhang et al., 2015; Wu et al., 2017). Also, the absolute values of both the slopes and corresponding standard deviations found here (0.80±0.04 and 1.00±0.06 for f(RH = 85%, 525 nm) as a function of inorganic and organic matter mass fractions, respectively) are similar to those reported in Lin'an, China (0.96±0.02 and 1.20±0.04, respectively; Zhang et al., 2015) but much lower than those observed at Melpitz, Germany (2.2±0.078 and 3.1±0.1, respectively; Zieger et al., 2014). It may be because the organic matter

220   mass concentrations of continental aerosols, like ambient aerosols measured at Lin'an and Beijing, were much higher than that of marine aerosols, while the inorganic matter mass concentrations were much lower.

Distinguishing between data points below and above the 40% organic mass fraction level in Fig. 6, the absolute values of the linear regression slope and R for data below 40% were lower than those for data above 40%. However, for the inorganic mass fraction (left panels of Fig. 6), the absolute values of the linear regression slope and R for data below 40% were higher than

225   those for data above 40%. This indicates that the positive correlation between f(RH = 85%, 525 nm) and the inorganic matter mass fraction was very strong when inorganic matter mass fractions were smaller than 40%. However, when inorganic matter mass fractions were larger than 40%, the increasing tendency in f(RH = 85%, 525 nm) as the proportion of inorganic matter increased slowly decreased. Inversely, the negative correlation between f(RH = 85%, 525 nm) and the organic matter mass fraction was slightly weak when organic matter mass fractions were smaller than 40%. When organic matter mass fractions

230   were larger than 40%, the decreasing tendency in f(RH = 85%, 525 nm) as the proportion of organic matter decreased became more robust. There may be several reasons for this phenomenon. First, particle size may be one of the most important factors to explain this. For particles with strong hygroscopicity, if their particle number size distribution (PNSD) tends towards large particle sizes, their hygroscopic growth ability may be similar to that of smaller particles with weak hygroscopicity (Y. Wang et al., 2017, 2018; Zieger et al., 2010). On the one hand, the f(RH) of aerosol particles (e.g., > 400 nm in diameter) usually

235   decreases with increasing particle size (Meier et al., 2009), resulting in a lower f(RH) for larger particles. On the other hand, the larger particles' amplification effect of scattering cross-section because of hygroscopic growth is weaker than that of smaller particles (Y. Wu et al., 2017). It may be that when there is a high proportion of inorganic matter and a low proportion of organic matter, the inorganic matter is mainly composed of relatively large particles. It is possible that the f(RH = 85%, 525 nm) of aerosols with a high level of inorganic matter and a low level of organic matter is not as high as expected due to the

240   compensating effect of aerosols. Second, the higher mass concentration of ambient aerosol maybe another reason. Overall, when the mass concentration of inorganic substances was less than 40%, the total mass concentration of aerosol was relatively low in this experiment. When the proportion of inorganic matter was higher than 40%, the total mass concentration of aerosol was high, with a clear inhibiting effect of high aerosol mass concentration to the f(RH = 85%, 525 nm) (Fig. 6e). Finally, it is also possible that when the proportion of inorganic matter is very high, the aerosol absorbs too much water vapor, leading to

245   insufficient ambient water vapor.

The green dots in the inset figures of Fig. 6a-d represent deliquescence. The range of inorganic mass fraction in these deliquescent processes was from 30% to 50%, and the range of organic mass fraction was from 40% to 60%). A comparison between Figs. 6a and 6c and Figs. 6b and 6d shows that the proportion of sulfate in the total aerosol was much higher than that

of nitrate for these deliquescent processes. Meanwhile, the f(RH = 85%, 525 nm) of these deliquescent processes were all

250 above the best-fit straight lines. This demonstrates that the scattering enhancement factor at 85% RH of deliquescence was

generally higher than that of the non-deliquescent process. Kuang et al. (2016) also draw the same conclusion.

Comparing Fig. 6a and Fig. 6c, as the proportion of inorganic salts in the total aerosol increased, the proportion of nitrate in

the total aerosol also increased, unlike the proportion of sulfate in the total aerosol. This demonstrates that nitrate played a

primary role in affecting aerosol hygroscopic enhancement during the study period in Beijing. Figure 7 also illustrates this.

255 Figures 7a-c show γ as a function of F_{org} (Eq. 7), where C_i represents SO_4^{2-}, NO_3^-, and the sum of SO_4^{2-} and NO_3^- mass

concentrations, respectively. Overall, γ and F_{org} are negatively correlated. The coefficient of determination between γ and

F_{org} (Org/(Org+NO_3^-)) (Fig. 7b) was higher than that between γ and F_{org} (Org/(Org+SO_4^{2-})) (Fig. 7a). The coefficient of

determination between γ and F_{org} (Org/(Org+NO_3^- + SO_4^{2-})) was the highest (Fig. 7c). This suggests that unlike the results

presented in previous studies (e.g., Malm et al., 2003; Pan et al., 2009; Quinn et al., 2005; Yan et al., 2009), the NO_3^- ion

260 played a more significant role than the SO_4^{2-} ion in affecting aerosol hygroscopic growth during the study period in Beijing.

Because the Chinese government has made more efforts to control SO_2 emissions, and desulfurization technology has already

been applied to many heavy industrial facilities in recent years, the decrease in SO_2 resulted in an increase in

NH_4NO_3 (Morgan et al., 2010; Xu et al., 2019). Several previous studies focused on megacities like Shanghai and Beijing have

all suggested that the increase in nitrate mass concentration played an important role in enhancing the water content of

265 submicron aerosols and reducing visibility under high RH conditions (Shi et al., 2014; Y. Sun et al., 2012; Zhang et al., 2015).

Figure S8a shows the scatterplot of γ as a function of F_{org} (Org/(Org+NO_3^- + SO_4^{2-})), where the color of the data points

represents the $SO_4^{2-}/(SO_4^{2-} + SO_2)$ molar ratio. This molar ratio indicates the relative age of aerosols (Quinn et al., 2005)

because by gas- and aqueous-phase oxidation processes, SO_2 will convert to SO_4^{2-}. The molar ratio of more aged aerosols is

high due to the sufficient time for the conversion. The $SO_4^{2-}/(SO_4^{2-} + SO_2)$ molar ratio is low for younger aerosols. The

270 figure shows that high γ corresponded to high $SO_4^{2-}/(SO_4^{2-} + SO_2)$ molar ratios with a low organic matter content, while

low γ corresponded to low $SO_4^{2-}/(SO_4^{2-} + SO_2)$ molar ratios with a high organic matter content, consistent with results

reported by Quinn et al. (2005) and Zhang et al. (2015). This demonstrates that the hygroscopicity of aged aerosols is higher

than that of younger aerosols. Figure S8b shows that the aerosol scattering coefficients $\log_{10}(\sigma_{sp})$ were relatively low when

γ was low, and the organic matter mass fraction was large. On the contrary, $\log_{10}(\sigma_{sp})$ was high when γ was high, and the

275 organic mass fraction was small, with a relatively large variation.

3.3 Deliquescence of ambient aerosols

Figure 8a shows the time series of η, with the color of the data points representing the ratio of SO_4^{2-} mass concentration to

NO_3^- mass concentration. Figures 8b and 8c show the time series of wind direction and wind speed, and ambient temperature

and RH, respectively. Overall, deliquescence often occurred under high ambient temperature and low RH conditions (Fig. 8c).

280 It also more easily occurred when wind with low speeds came from the south or southwest (Fig. 8b). High values of η usually

occurred when the ratio of SO_4^{2-} mass concentration to NO_3^- mass concentration was high (mostly higher than ~4). Figure 9a shows a relatively strong correlation between η and the ratio of SO_4^{2-} mass concentration to NO_3^- mass concentration ($R_1 = 0.62$). The blue dots represent the hysteresis index ($\eta > 0.4$) of deliquescence and show that the corresponding ratios of SO_4^{2-} mass concentration to NO_3^- mass concentration were high (mostly higher than ~4). The red dots represent the

285 hysteresis index of non-deliquescent processes, showing that the corresponding ratios of SO_4^{2-} mass concentration to NO_3^- mass concentration were generally less than 4. Because $PM_{2.5}$ mass concentrations were extremely low on 24 September 2019, data were noisy then, and the system error was relatively large (green dots). When these cases of large systematic errors were eliminated, the correlation between η and the ratio of SO_4^{2-} to NO_3^- mass concentration increased ($R_2 = 0.69$). In the North China Plain, Kuang et al. (2016) also observed a similar deliquescent phenomenon associated with ammonium sulfate, while in Ny-Ålesunf, Norway, this deliquescent phenomenon was related to sea salt (Zieger et al., 2010).

According to observational results, there are two environmental conditions of consequence for ambient aerosol deliquescence:

1. High ambient temperature and low ambient RH;

2. Relatively good air quality and solar illumination.

Concerning the first condition, Cheung et al. (2015) proposed an indicator describing the neutralization extent of aerosols, i.e.,

295 the molar ratio, $MR = (NH_4^+ - NO_3^-)/SO_4^{2-}$. The MR value of the non-deliquescent process was always the lowest in their study. Their results indicate that when the nitrate content of ambient aerosols was slightly high, and the sulfate content was low, aerosol particles did not exhibit deliquescence resulting from acidic sulfate. Here, only when the mass concentration ratio of sulfate to nitrate was high (mostly higher than ~4) did ambient aerosol particles exhibit deliquescence. Figures 10a and 10b illustrate the diurnal variation in nitrate, along with ammonium and sulfate. Both the mass concentration and mass fraction of

300 nitrate reached their largest and smallest values in the early morning and in the afternoon, respectively. It was closely correlated with the diurnal variation in ambient temperature and RH, where RH gradually rose as the temperature gradually decreased from the late afternoon to the early morning of the next day, followed by a reversal of the trend into the late afternoon of the next day (Fig. 8c). Morino et al. (2006) and X. Wang et al. (2009) found that the formation of nitrate requires low temperature and high RH, conditions favorable for the conversion of gaseous nitric acid to solid-phase nitrate. Ambient aerosol

305 deliquescence is thus closely related to the environmental conditions of high temperature and low humidity. Note that secondary sulfates are usually produced by photochemical reactions so that the sulfate content of aerosols gradually accumulates from late morning to late afternoon (Huang et al., 2010; Y. Sun et al., 2012). Generally speaking, the ambient temperature was higher, and the humidity was lower in the afternoon (Fig. 4e), so high values of SO_4^{2-}/NO_3^- mostly occurred in the afternoon. This may also explain why the deliquescent cycle occurred most frequently in the afternoon, as shown in Fig.

310 9b.

Concerning the second condition, the blue-shaded zones in Figs. 2a and 2f show that deliquescence usually occurred when the air quality was good. To better explain this phenomenon, the observation period was divided into a very clean period ($PM_{2.5} \leqslant 35\ \mu g\ m^{-3}$) and a moderately polluted period ($PM_{2.5} > 75\ \mu g\ m^{-3}$). Figure 10c shows the diurnal variation of the difference

Atmospheric
Chemistry
and Physics
Discussions

Open Access

EGU

between f(RH = 85%, 525 nm) and f(RH = 80%, 525 nm) (DF) during a very clean period and a moderately polluted period.

315   The DF of deliquescence is larger than that of non-deliquescence because the f(RH) of deliquescence jumps suddenly as the RH increases from 80% to 85%, while the f(RH) of non-deliquescence increases smoothly as the RH increases. The values of the hygroscopic enhancement factor at high RH for deliquescent processes were usually higher than that for non-deliquescent processes, consistent with the strong hygroscopicity of ammonium sulfate. Figure 10c shows the diurnal range of DF during the clean period was larger than that during the moderately polluted period. In particular, from late morning to late afternoon,

320   the DF during the clean period was much higher than that during the moderately polluted period. Figure 10d shows the diurnal variation of SO_4^{2-}/NO_3^-. The ratio SO_4^{2-}/NO_3^- during the clean period was higher than that during the moderately polluted period, especially from late morning to late afternoon. Overall, good air quality and solar illumination were conducive to photochemical reactions so that more secondary sulfate could be generated during the day, facilitating the deliquescence of ambient aerosols.

3.4 Parameterizations of f(RH)

3.4.1 Parameterization with the equation $f(\mathrm{RH}) = 1 + \mathrm{m} \times RH^n$

Many empirical expressions have been presented to depict f(RH) (Brock et al., 2016; Carrico et al., 2003; Chen et al., 2014; Fierz-Schmidhauser et al., 2010a; Kotchenruther and Hobbs, 1998; Kuang et al., 2017; Pan et al., 2009; Titos et al., 2016). The following is the two-parameter scheme introduced by Kotchenruther and Hobbs (1998):

330     $$f(\mathrm{RH}) = 1 + m \times \mathrm{RH}^n. \tag{10}$$

The parameter m determines the largest value of f(RH = 100%), and the parameter n dominates the magnitude of the scattering enhancement and reflects the curvature of the humidogram.

Deliquescence was frequently observed during the entire measurement campaign. In total, 294 cycles of f(RH) were measured, and 47 cycles (16% of all cycles) showed clear deliquescence (Figs. 11d and 11e). All f(RH) curves were thus first classified

335   into deliquescent curves and non-deliquescent curves. After averaging $PM_{2.5}$ concentrations of the corresponding cycles, all non-deliquescent curves were further divided into clean ($PM_{2.5} \leq 35$ μg m^{-3}), moderately polluted (35 μg m^{-3} < $PM_{2.5} \leq$ 75 μg m^{-3}), and polluted ($PM_{2.5} > 75$ μg m^{-3}) categories. The deliquescent curves were divided into clean and moderately clean categories only because deliquescence mainly occurred under good air quality conditions. For cycles without deliquescence (Figs. 11a, 11b, and 11c), the measured values were fitted using Eq. (10). For cycles with deliquescence (Figs. 11d and 11e),

340   f(RH) increased smoothly under low RH conditions then increased sharply. Under low and high RH conditions, the fitted f(RH) values were usually lower than observed values, but the slopes of the two curves were similar. However, when RH approached ~80% where f(RH) sharply increased, the fitted f(RH) values were usually higher than observed values, with different slopes of the two curves. Therefore, segment fitting (Eq. (12)) was applied in the parameterization of deliquescent f(RH). The deliquescence observed in our study was primarily caused by ammonium sulfate in ambient aerosols. The deliquescence RH

345   (DRH) of the pure ammonium sulfate aerosols generated in the laboratory was 80.367%, measured by our high-resolution

humidified nephelometer system (Fig. S8). Because the DRH of all deliquescence in this study, according to statistics, was

mainly distributed between 78% and 80%, Eq. (10) was applied to fit f(RH) values when RH $\geqslant$ 82% or RH $\leqslant$ 78%, and

for 78% < RH < 82%, f(RH) values were parameterized by Eq. (11):

$$f(\mathrm{RH}) = a \times \mathrm{RH} + b. \tag{11}$$

350   Parameter a determines the degree of f(RH) jumps during deliquescence, i.e., the slope of the linear fitting line. Parameter b

determines the f(RH, 525 nm) value before deliquescence (RH = 78%) and after deliquescence (RH = 82%).

$$\begin{cases} f(\mathrm{RH}) = 1 + m \times \mathrm{RH}^n & \mathrm{RH} \leq 78\% \\ f(\mathrm{RH}) = a \times \mathrm{RH} + b & 78\% < \mathrm{RH} < 82\% \\ f(\mathrm{RH}) = 1 + m \times \mathrm{RH}^n & \mathrm{RH} \geq 82\% \end{cases} \tag{12}$$

Table 2 summarizes the parameters m and n used in this study and in similar studies. For the non-deliquescence case, the

parameter n for the clean period was the largest (~27% larger than that for the moderately polluted period and ~16% larger

355   than that for the polluted period). The difference between the clean and moderately polluted parameter m was small, while the

parameter m in the polluted period was about 0.1 larger than that in the other two periods. As a result, f(RH = 85%, 525 nm)

was the largest in the polluted period and the smallest in the clean period. For the deliquescence case, the fitted parameters m

and n for the whole RH range (40% < RH < 90%) were much larger than the m and n for RH < 78% and slightly larger than

the m and n for RH > 82%. If Eq. (10) was used to parameterize the whole RH range of the deliquescence curves instead of

360   segment fitting, bigger differences between the parameterized fitting results and measured values would occur. This would

cause greater uncertainties in the model simulation of aerosol hygroscopicity. Also, there was no significant difference between

parameter a under clean (a = 0.07±0.006) and moderately polluted (a = 0.07±0.003) conditions, indicating that the trend and

amplitude of the jump growth for aerosol deliquescence are consistent under these two environmental conditions. However,

the absolute value of parameter b under clean conditions (b = -4.29±0.47) was higher than that under moderately polluted

365   conditions (b = -3.88±0.24), indicating that the DRH for clean periods was slightly higher than that for moderately polluted

periods.

3.4.2 Steepness of humidograms

The steepness index, τ, defined as

$$\tau = \frac{f'(80\%)}{f'(60\%)} - 1 = \left(\frac{4}{3}\right)^{n-1} - 1, \tag{13}$$

370   was applied to quantitatively describe the patterns of the humidogram curves generated in this study. In Eq. (13), $f'(80\%)$

and $f'(60\%)$ represent the derivatives of every fitting curve at the corresponding RH and f(RH) fitted by Eq. (10).

A low τ means that the curvature of the humidogram is small, and a high τ means that the slopes of the curve from low to high RH sharply change. Figure 12 shows the scatter plot of τ as a function of the nitrate mass fraction, colored by the sulfate mass fraction. In the 0–15% nitrate mass fraction range, τ decreased sharply as the nitrate mass fraction increased, demonstrating

375   that the curvature of the humidogram became smaller. For nitrate mass fractions larger than 15%, τ stabilized to a constant value of ~1.6, and the curvature of the humidogram was much smaller.

4 Conclusions

Direct measurements of aerosol hygroscopicity as expressed by $f(\mathrm{RH}, \lambda)$ was carried out at a site in a southern urban edge of Beijing, aimed at investigating the effect of aerosol water uptake on particle light-scattering properties. The mass

380   concentrations of aerosol chemical compositions were measured simultaneously by the ACSM and AE-33. Also measured were other aerosol parameters such as the light absorption coefficient and the mass concentration of $\mathrm{PM}_{2.5}$. In total, 294 cycles of f(RH) were measured, and 47 cycles (16% of all cycles) showed clear deliquescence.

The proportion of components making up the chemical composition of aerosols is key to influencing f(RH). In general, f(RH) had a strong positive correlation with the proportion of inorganic matter and a negative correlation with the proportion of

385   organic matter and BC. High values of f(RH) usually occurred for aged aerosols whose mass fraction of organic matter was small. Low values of f(RH = 85%, 525 nm) often occurred for primary aerosols of more organic matter. Furthermore, when the mass fraction of inorganic matter was smaller than 40%, the positive correlation between f(RH = 85%, 525 nm) and the inorganic matter was much stronger. A similar phenomenon was also found for the negative correlation between the organic matter and f(RH = 85%, 525 nm). The compensating effect of aerosol may be one of the main reasons for this phenomenon.

390   High mass concentration of ambient aerosol and insufficient water vapor in sample flow may be the other two reasons. Besides, nitrate played a more significant role in affecting aerosol hygroscopic growth than sulfate in Beijing.

Favorable meteorological conditions for aerosol deliquescence were high ambient temperature and low RH, and relatively good air quality and strong solar illumination. High temperatures and low RH levels were not conducive to the formation of nitrate, while good air quality and light conditions were conducive to photochemical reactions so that more secondary sulfate

395   could be generated. Only when the ratio of the sulfate mass fraction to the nitrate mass fraction was greater than ~4 did the deliquescence phenomenon of ambient aerosols easily occur.

All humidograms were first classified as either deliquescent or non-deliquescent. Two kinds of humidograms were further classified according to the mass concentration of $\mathrm{PM}_{2.5}$. The two-parameter scheme, $f(\mathrm{RH}) = 1 + m \times \mathrm{RH}^n$, introduced by Kotchenruther and Hobbs (1998), was applied to fit the non-deliquescent f(RH), while the deliquescent f(RH) was

400   parameterized by segment functions (Eq. (12)). For the deliquescence case, the fitted parameters m and n for the whole RH range (40% < RH < 90%) were much larger than the parameters for RH < 78% and higher than the parameters for RH > 82%. This demonstrates that large errors will be incurred if only Eq. (10) was used to parameterize the whole RH range of deliquescence curves. The piecewise parameterized scheme (Eq. (12)) is a better fit for the humidograms of the deliquescence

405   case to reduce uncertainties in the model simulation of aerosol hygroscopicity. The curvature of the f(RH) humidogram, described by the steepness index, decreased sharply as the nitrate mass fraction increased within the range of 0–15%. When the nitrate mass fraction was larger than 15%, the steepness index remained constant (~1.6).

Data availability.

The data used in this manuscript can be downloaded online (website: https://pan.baidu.com/s/1aE6mvkhSSbQ5mTyIOLgvng; password: 1370).

410   **Author contributions.**

ZL and PY designed the field experiment. ZL, PY, and RR determined the main goal of this study. RR processed the measurement data and prepared this paper with contributions from all co-authors. PY, HW, and YW provided technical guidance for instrumentation. MC copyedited the article. Other co-authors participated in the implementation of this experiment.

415   **Competing interests.**

The authors declare that they have no conflict of interest.

Acknowledgement.

References

Bond, T. C., and Bergstrom, R. W.: Light absorption by carbonaceous particles: an investigative review, Aerosol Sci. Tech., 40, 27–67, https://doi.org/10.1080/02786820500421521, 2006.

Brock, C. A., Wagner, N. L., Anderson, B. E., Attwood, A. R., Beyersdorf, A., Campuzano-Jost, P., Carlton, A. G., Day, D. A.,
425   Diskin, G. S., Gordon, T.D., Jimenez, J. L., Lack, D. A., Liao, J., Markovic, M. Z., Middlebrook, A. M., Ng, N. L., Perring, A. E., Richardson, M. S., Schwarz, J. P., Washenfelder, R. A., Welti, A., Xu, L., Ziemba, L. D., and Murphy, D. M.: Aerosol optical properties in the southeastern United States in summer – Part 1: Hygroscopic growth, Atmos. Chem. Phys., 16, 4987–5007, https://doi.org/10.5194/acp-16-4987-2016, 2016.

Atmospheric
Chemistry
and Physics
Discussions

430 Carrico, C. M., Rood, M. J., and Ogren, J. A.: Aerosol light scattering properties at Cape Grim, Tasmania, during the First Aerosol Characterization Experiment (ACE 1), J. Geophys. Res. Atmos., 103, 16,565–16,574, https://doi.org/10.1029/98JD00685, 1998.

Carrico, C. M., Kus, P., Rood, M. J., Quinn, P. K., and Bates, T. S.: Mixtures of pollution, dust, sea salt, and volcanic aerosol during ACE-Asia: radiative properties as a function of relative humidity, J. Geophys. Res. Atmos., 108, 8650, https://doi.org/10.1029/2003JD003405, 2003.

435 Chen, J., Zhao, C., Ma, N., and Yan, P.: Aerosol hygroscopicity parameter derived from the light scattering enhancement factor measurements in the North China Plain, Atmos. Chem. Phys., 14, 8105-8118, https://doi.org/10.5194/acp-14-8105-2014, 2014.

Chen, J., Li, Z., Lv, M., Wang, Y., Wang, W., Zhang, Y., Wang, H., Yan, X., Sun, Y., and Cribb, M.: Aerosol hygroscopic growth, contributing factors, and impact on haze events in a severely polluted region in northern China, Atmos. Chem. Phys., 440 19, 1327–1342, https://doi.org/10.5194/acp-19-1327-2019, 2019.

Cheung, H. H. Y., Yeung, M. C., Li, Y. J., Lee, B. P., and Chan, C. K.: Relative humidity-dependent TDMA measurements of ambient aerosols at the HKUST supersite in Hong Kong, China, Aerosol Sci. Tech., 49, 643–654, https://doi.org/10.1080/02786826.2015.1058482, 2015.

Deng, H., Tan, H., Li, F., Cai, M., Chan, P. W., Xu, H., Huang, X., and Wu, D.: Impact of relative humidity on visibility 445 degradation during a haze event: A case study, Sci. Total Environ., 569-570, 1149-1158, https://doi.org/10.1016/j.scitotenv.2016.06.190, 2016.

Doherty, S. J., Quinn, P. K., Jefferson, A., Carrico, C. M., Anderson, T. L., and Hegg, D.: A comparison and summary of aerosol optical properties as observed in situ from aircraft, ship, and land during ACE-Asia, J. Geophys. Res. Atmos., 110, D04201, https://doi.org/10.1029/2004jd004964, 2005.

450 Fierz-Schmidhauser, R., Zieger, P., Gysel, M., Kammermann, L., Decarlo, P. F., Baltensperger, U., and Weingartner, E.: Measured and predicted aerosol light scattering enhancement factors at the high alpine site Jungfraujoch, Atmos. Chem. Phys., 10, 2319–2333, https://doi.org/10.5194/acp-10-2319-2010, 2010a.

Fierz-Schmidhauser, R., Zieger, P., Wehrle, G., Jefferson, A., Ogren, J. A., Baltensperger, U., and Weingartner, E.: Measurement of relative humidity dependent light scattering of aerosols, Atmos. Meas. Tech., 3, 39–50, 455 https://doi.org/10.5194/amt-3-39-2010, 2010b.

Han, T., Xu, W., Chen, C., Liu, X., Wang, Q., Li, J., Zhao, X., Du, W., Wang, Z., and Sun, Y.: Chemical apportionment of aerosol optical properties during the Asia-Pacific Economic Cooperation summit in Beijing, China, J. Geophys. Res. Atmos., 120, 12,281–12,295, https://doi.org/10.1002/2015JD023918, 2015.

Huang, X. F., He, L. Y., Hu, M., Canagaratna, M. R., Sun, Y., Zhang, Q., Zhu, T., Xue, L., Zeng, L. W., Liu, X. G., Jayne, J. 460 T., Ng, N. L., and Worsnop, D. R.: Highly time-resolved chemical characterization of atmospheric submicron

particles during 2008 Beijing Olympic Games using an Aerodyne high-resolution aerosol mass spectrometer, Atmos. Chem. Phys., 10, 8933–8945, https://doi.org/10.5194/acpd-10-13219-2010, 2010.

IPCC: Climate Change 2013: The Physical Science Basis. Cambridge University Press, Cambridge, United Kingdom and New York, NY, USA, 2013.

465 Jin, X., Wang, Y., Li, Z., Zhang, F., Xu, W., Sun, Y., Fan, X., Chen, G., Wu, H., Ren, J., Wang, Q., and Cribb, M.: Significant contribution of organics to aerosol liquid water content in winter in Beijing, China, Atmos. Chem. Phys., 20, 901–914, https://doi.org/10.5194/acp-20-901-2020, 2020.

Kotchenruther, R. A., and Hobbs, P. V.: Humidification factors of aerosols from biomass burning in Brazil, J. Geophys. Res. Atmos., 103, 32,081–32,089, https://doi.org/10.1029/98JD00340, 1998.

470 Kuang, Y., Zhao, C. S., Ma, N., Liu, H. J., Bian, Y. X., Tao, J. C., and Hu, M.: Deliquescent phenomena of ambient aerosols on the North China Plain, Geophys. Res. Lett., 43, 8744–8750, https://doi.org/10.1002/2016gl070273, 2016.

Kuang, Y., Zhao, C., Tao, J., Bian, Y., Ma, N., and Zhao, G.: A novel method for deriving the aerosol hygroscopicity parameter based only on measurements from a humidified nephelometer system, Atmos. Chem. Phys., 17, 6651–6662, https://doi.org/10.1002/2016GL070273, 2017.

475 Li, Z., Wang, Y., Guo, J., Zhao, C., Cribb, M. C., Dong, X., Fan, J., Gong, D., Huang, J., Jiang, M., Jiang, Y., Lee, S.-S., Li, H., Li, J., Liu, J., Qian, Y., Rosenfeld, D., Shan, S., Sun, Y., Wang, H., Xin, J., Yan, X., Yang, X., Yang, X.-q., Zhang, F., and Zheng, Y.: East Asian Study of Tropospheric Aerosols and their Impact on Regional Clouds, Precipitation, and Climate (EAST-AIRCPC), J. Geophys. Res. Atmos., 124, 13,026–13,054, https://doi.org/10.1029/2019jd030758, 2019.

480 Liu, C., Chung, C. E., Yin, Y., and Schnaiter, M.: The absorption Angstrom exponent of black carbon: from numerical aspects, Atmos. Chem. Phys., 18, 6259–6273, https://doi.org/10.5194/acp-18-6259-2018, 2018.

Liu, H., and Zhao, C.: Design of a Humidified Nephelometer System with High Time Resolution, Acta Scientiarum Naturalium Universitatis Pekinensis, 52, 999–1004, https://doi.org/10.13209/j.0479-8023.2016.053, 2016.

Liu, L., Tan, H., Fan, S., Cai, M., Xu, H., Li, F., and Chan, P.: Influence of aerosol hygroscopicity and mixing state on aerosol
485 optical properties in the Pearl River Delta region, China, Sci. Total Environ., 627, 1560–1571, https://doi.org/10.1016/j.scitotenv.2018.01.199, 2018.

Liu, X. G., Li, J., Qu, Y., Han, T., Hou, L., Gu, J., Chen, C., Yang, Y., Liu, X., Yang, T., Zhang, Y., and Tian, H.: Formation and evolution mechanism of regional haze: a case study in the megacity Beijing, China, Atmos. Chem. Phys., 13, 4501–4514, https://doi.org/10.5194/acp-13-4501-2013, 2013.

490 Malm, W. C., Day, D. E., Kreidenweis, S. M., Collett, J. L., and Lee, T.: Humidity-dependent optical properties of fine particles during the Big Bend Regional Aerosol and Visibility Observational Study, J. Geophys. Res. Atmos., 108, 4279, https://doi.org/10.1029/2002JD002998, 2003.

Meier, J., Wehner, B., Massling, A., Birmili, W., Nowak, A., Gnauk, T., Brüggemann, E., Herrmann, H., Min, H., and Wiedensohler, A.: Hygroscopic growth of urban aerosol particles in Beijing (China) during wintertime: a comparison

495   of three experimental methods, Atmos. Chem. Phys., 9, 6865–6880, https://doi.org/10.5194/acpd-9-6889-2009, 2009.

Morgan, W. T., Allan, J. D., Bower, K. N., Esselborn, M., Harris, B., Henzing, J. S., Highwood, E. J., Kiendlerscharr, A., Mcmeeking, G. R., Mensah, A. A., Northway, M. J., Osborne, S., Williams, P. I., and Krejci, R.: Enhancement of the aerosol direct radiative effect by semi-volatile aerosol components: airborne measurements in North-Western Europe, Atmos. Chem. Phys., 10, 8151–8171, https://doi.org/10.5194/acp-10-8151-2010, 2010.

500 Morino, Y., Kondo, Y., Takegawa, N., Miyazaki, Y., Kita, K., Komazaki, Y., Fukuda, M., Miyakawa, T., Moteki, N., and Worsnop, D. R.: Partitioning of HNO_3 and particulate nitrate over Tokyo: effect of vertical mixing, J. Geophys. Res. Atmos., 111, D15215, https://doi.org/10.1029/2005jd006887, 2006.

Pan, X. L., Yan, P., Tang, J., Ma, J. Z., Wang, Z. F., and Gbaguidi, A.: Observational study of aerosol hygroscopic growth factors over rural area near Beijing megacity, Atmos. Chem. Phys., 9, 5087–5118, https://doi.org/10.5194/acpd-9-

505   5087-2009, 2009.

Quinn, P. K., Bates, T. S., Baynard, T., Clarke, A. D., Onasch, T. B., Wang, W., Rood, M. J., Andrews, E., Allan, J., Carrico, C. M., Coffman, D., and Worsnop, D.: Impact of particulate organic matter on the relative humidity dependence of light scattering: a simplified parameterization, Geophys. Res. Lett., 32, L22809, https://doi.org/10.1029/2005gl024322, 2005.

510 Shi, Y., Chen, J., Hu, D., Wang, L., Yang, X., and Wang, X.: Airborne submicron particulate (PM_1) pollution in Shanghai, China: chemical variability, formation/dissociation of associated semi-volatile components and the impacts on visibility, Sci. Total Environ., 473–474, 199–206, https:// doi.org/10.1016/j.scitotenv.2013.12.024, 2014.

Sun, Y., Wang, Z., Dong, H., Yang, T., Li, J., Pan, X., Chen, P., and Jayne, J. T.: Characterization of summer organic and inorganic aerosols in Beijing, China with an aerosol chemical speciation monitor, Atmos. Environ., 51, 250–259,

515   https://doi.org/10.1016/j.atmosenv.2012.01.013, 2012.

Titos, G., Cazorla, A., Zieger, P., Andrews, E., Lyamani, H., Granadosmunoz, M. J., Olmo, F. J., and Aladosarboledas, L.: Effect of hygroscopic growth on the aerosol light-scattering coefficient: a review of measurements, techniques and error sources, Atmos. Environ., 141, 494–507, https://doi.org/10.1016/j.atmosenv.2016.07.021, 2016.

Wang, X., Zhang, Y., Chen, H., Yang, X., Chen, J., and Geng, F.: Particulate nitrate formation in a highly polluted urban area:

520   a case study by single-particle mass spectrometry in Shanghai, Environ. Sci. Technol., 43, 3061–3066, https://doi.org/10.1021/es8020155, 2009.

Wang, Y., Zhang, F., Li, Z., Tan, H., Xu, H., Ren, J., Zhao, J., Du, W., and Sun, Y.: Enhanced hydrophobicity and volatility of submicron aerosols under severe emission control conditions in Beijing, Atmos. Chem. Phys., 17, 5239–5251, https://doi.org/10.5194/acp-17-5239-2017, 2017.
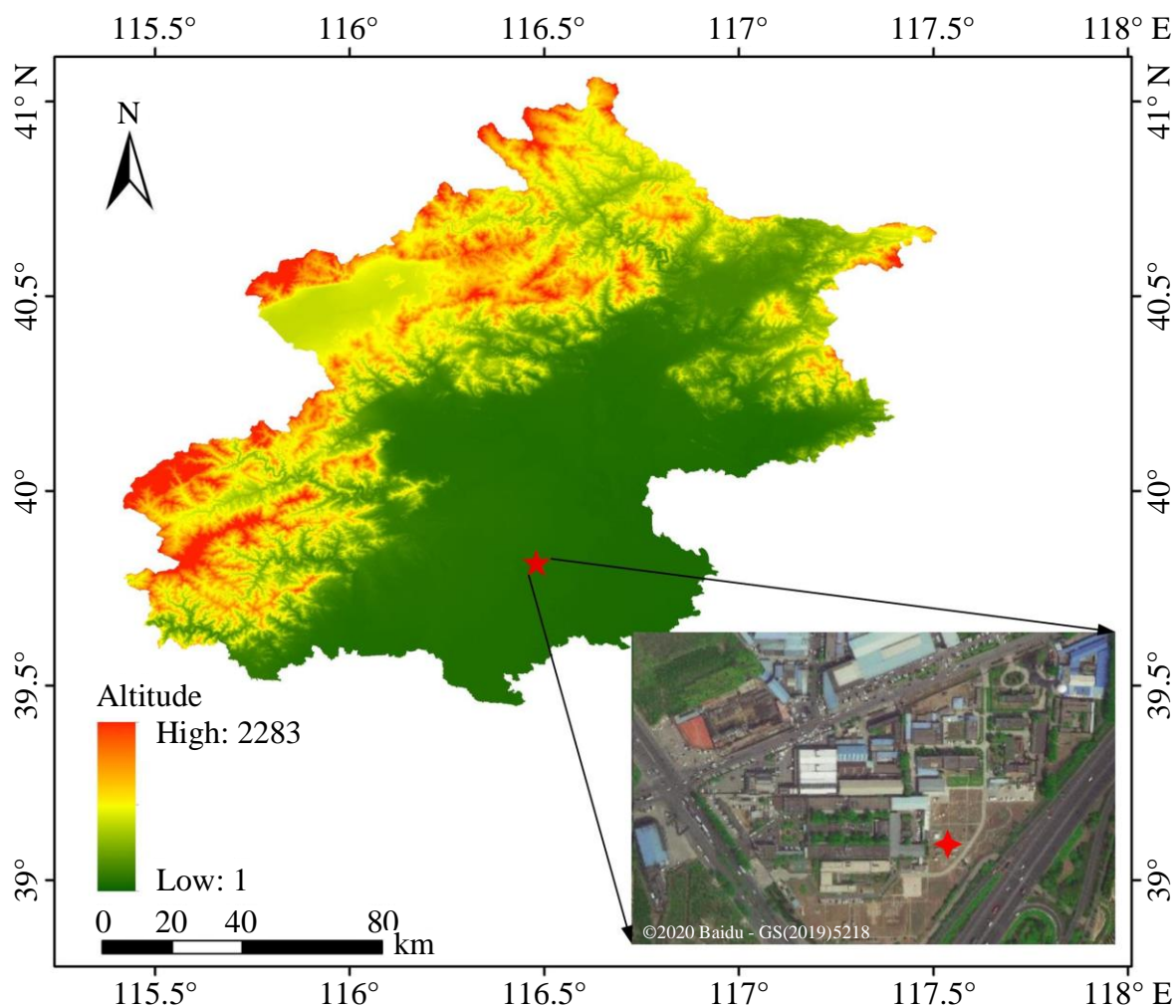
Atmospheric
Chemistry
and Physics
Discussions

525 Wang, Y., Li, Z., Zhang, Y., Du, W., Zhang, F., Tan, H., Xu, H., Fan, T., Jin, X., Fan, X., Dong, Z., Wang, Q., and Sun, Y.: Characterization of aerosol hygroscopicity, mixing state, and CCN activity at a suburban site in the central North China Plain, Atmos. Chem. Phys., 18, 11,739–11,752, https://doi.org/10.5194/acp-18-11739-2018, 2018.

Wang Y., Li, Z., Zhang, R., Jin, X., Xu, W., Fan, X., Wu, H., Zhang, F., Sun, Y., Wang, Q., Cribb, M., and Hu, D.: Distinct ultrafine-and accumulation-mode particle properties in clean and polluted urban environments, Geophys. Res. Lett., 530 46, 10,918–10,925, https://doi.org/10.1029/2019GL084047, 2019.

Wu, T., Li, Z., Chen, J., Wang, Y., Wu, H., Jin, X., Liang, C., Li, S., Wang, W., and Cribb, M.: Hygroscopicity of different types of aerosol particles: case studies using multi-instrument data in megacity Beijing, China, Remote Sens., 12, 785, https://doi.org/10.3390/rs12050785, 2020.

Wu, Y., Wang, X., Yan, P., Zhang, L., Tao, J., Liu, X., Tian, P., Han, Z., and Zhang, R.: Investigation of hygroscopic growth 535 effect on aerosol scattering coefficient at a rural site in the southern North China Plain, Sci. Total Environ., 599–600, 76–84, https://doi.org/10.1016/j.scitotenv.2017.04.194, 2017.

Xu, W., Sun, Y., Wang, Q., Zhao, J., Wang, J., Ge, X., Xie, C., Zhou, W., Du, W., Li, J., Fu, P., Wang, Z., Worsnop, D. R., Coe, H.: Changes in aerosol chemistry from 2014 to 2016 in winter in Beijing: insights from high-resolution aerosol mass spectrometry, J. Geophys. Res. Atmos., 124, 1132–1147, https://doi.org/10.1029/2018JD029245, 2019.

540 Yan, P., Pan, X., Tang, J., Zhou, X., Zhang, R., and Zeng, L.: Hygroscopic growth of aerosol scattering coefficient：a comparative analysis between urban and suburban sites at winter in Beijing, Particuology, 7, 52–60, https://doi.org/10.1016/j.partic.2008.11.009, 2009.

Yang, Y., Liu, X., Qu, Y., An, J., Jiang, R., Zhang, Y., Sun, Y., Wu, Z., Zhang, F., Xu, W., and Ma, Q.: Characteristics and formation mechanism of continuous hazes in China: a case study during the autumn of 2014 in the North China 545 Plain, Atmos. Chem. Phys., 15, 8165–8178, https://doi.org/10.5194/acp-15-8165-2015, 2015.

Yu, Y., Zhao, C., Kuang, Y., Tao, J., Zhao, G., Shen, C., and Xu, W.: A parameterization for the light scattering enhancement factor with aerosol chemical compositions, Atmos. Environ., 191, 370–377, https://doi.org/10.1016/j.atmosenv.2018.08.016, 2018.

Zhang, L., Sun, J., Shen, X., Zhang, Y., Che, H. C., Ma, Q., Zhang, Y., Zhang, X., and Ogren, J. A.: Observations of relative 550 humidity effects on aerosol light scattering in the Yangtze River Delta of China, Atmos. Chem. Phys., 15, 8439–8454, https://doi.org/10.5194/acp-15-8439-2015, 2015.

Zhao, C., Yu, Y., Kuang, Y., Tao, J., and Zhao, G.: Recent progress of aerosol light-scattering enhancement factor studies in China, Adv. Atmos. Sci., 36, 1015–1026, https://doi.org/10.1007/s00376-019-8248-1, 2019.

Zhao, G., Zhao, C., Kuang, Y., Bian, Y., Tao, J., Shen, C., and Yu, Y.: Calculating the aerosol asymmetry factor based on 555 measurements from the humidified nephelometer system, Atmos. Chem. Phys., 18, 9049–9060, https://doi.org/10.5194/acp-18-9049-2018, 2018.

Zhao, P., Ding, J., Du, X., and Su, J.: High time-resolution measurement of light scattering hygroscopic growth factor in Beijing: a novel method for high relative humidity conditions, Atmos. Environ., 215, 116912, https://doi.org/10.1016/j.atmosenv.2019.116912, 2019.

560 Zieger, P., Fierz-Schmidhauser, R., Gysel, M., Ström, J., Henne, S., Yttri, K. E., Baltensperger, U., and Weingartner, E.: Effects of relative humidity on aerosol light scattering in the Arctic, Atmos. Chem. Phys., 10, 3875–3890, https://doi.org/10.5194/acp-10-3875-2010, 2010.

Zieger, P., Fierz-Schmidhauser, R., Poulain, L., Müller, T. J., Birmili, W., Spindler, G., Wiedensohler, A., Baltensperger, U., and Weingartner, E.: Influence of water uptake on the aerosol particle light-scattering coefficients of the Central
565 European aerosol, Tellus B., 66, 22716, http://dx.doi.org/10.3402/tellusb.v66.22716, 2014.

Zou, J., Yang, S., Hu, B., Liu, Z., Gao, W., Xu, H., Du, C., Wei, J., Ma, Y., Ji, D., and Wang, Y.: A closure study of aerosol optical properties as a function of RH using a κ-AMS-BC-Mie model in Beijing, China, Atmos. Environ., 197, 1–13, https://doi.org/10.1016/j.atmosenv.2018.10.015, 2019.

570

Figure 1: Map of the terrain heights of Beijing, China (unit: m above sea level). The red star shows the position of the observatory, and the image in the lower right corner is a true-color image of the observatory surroundings.
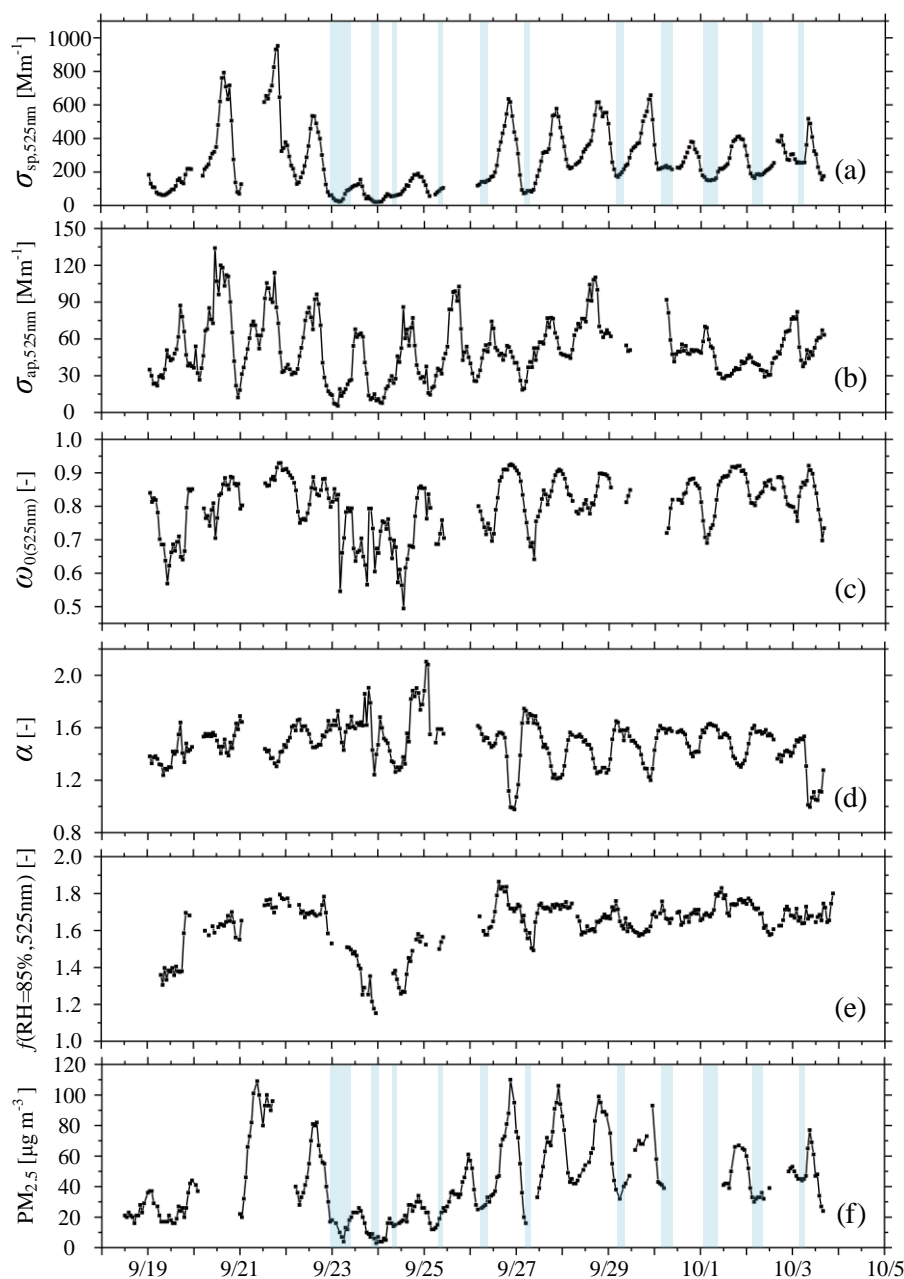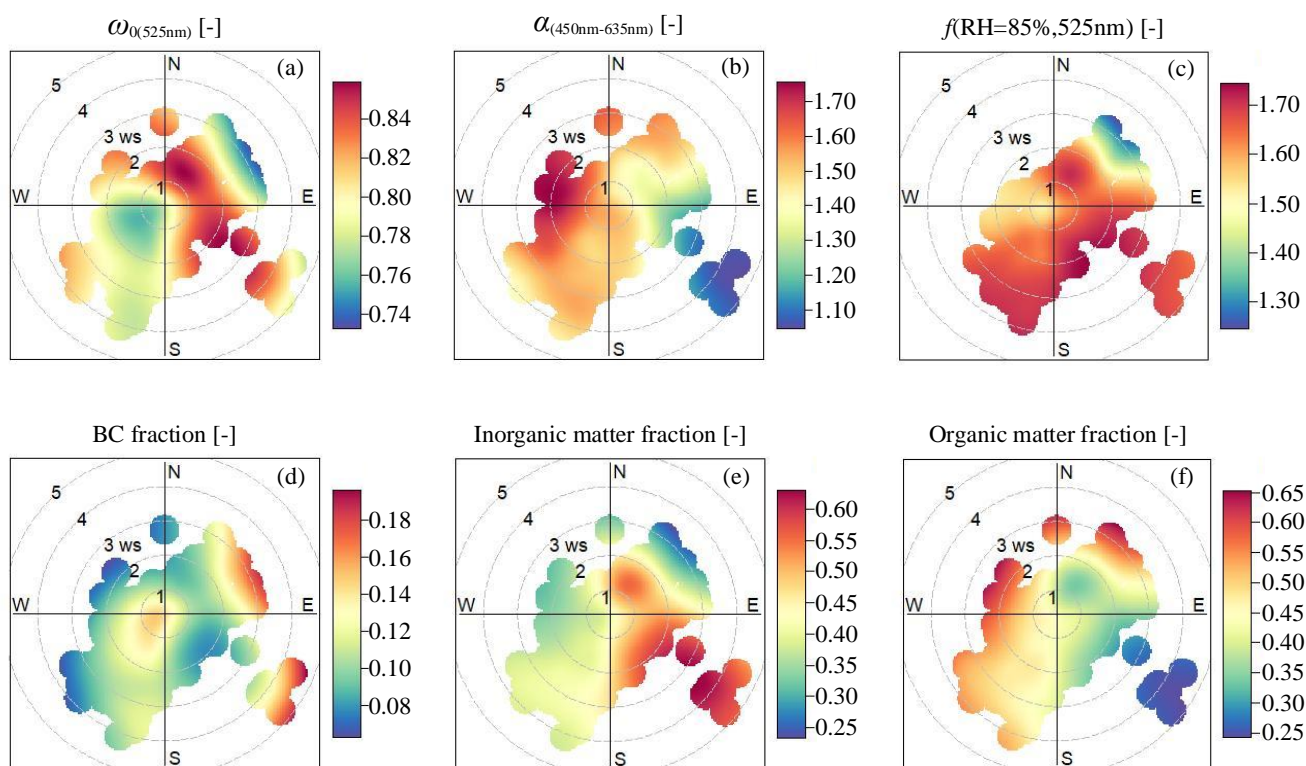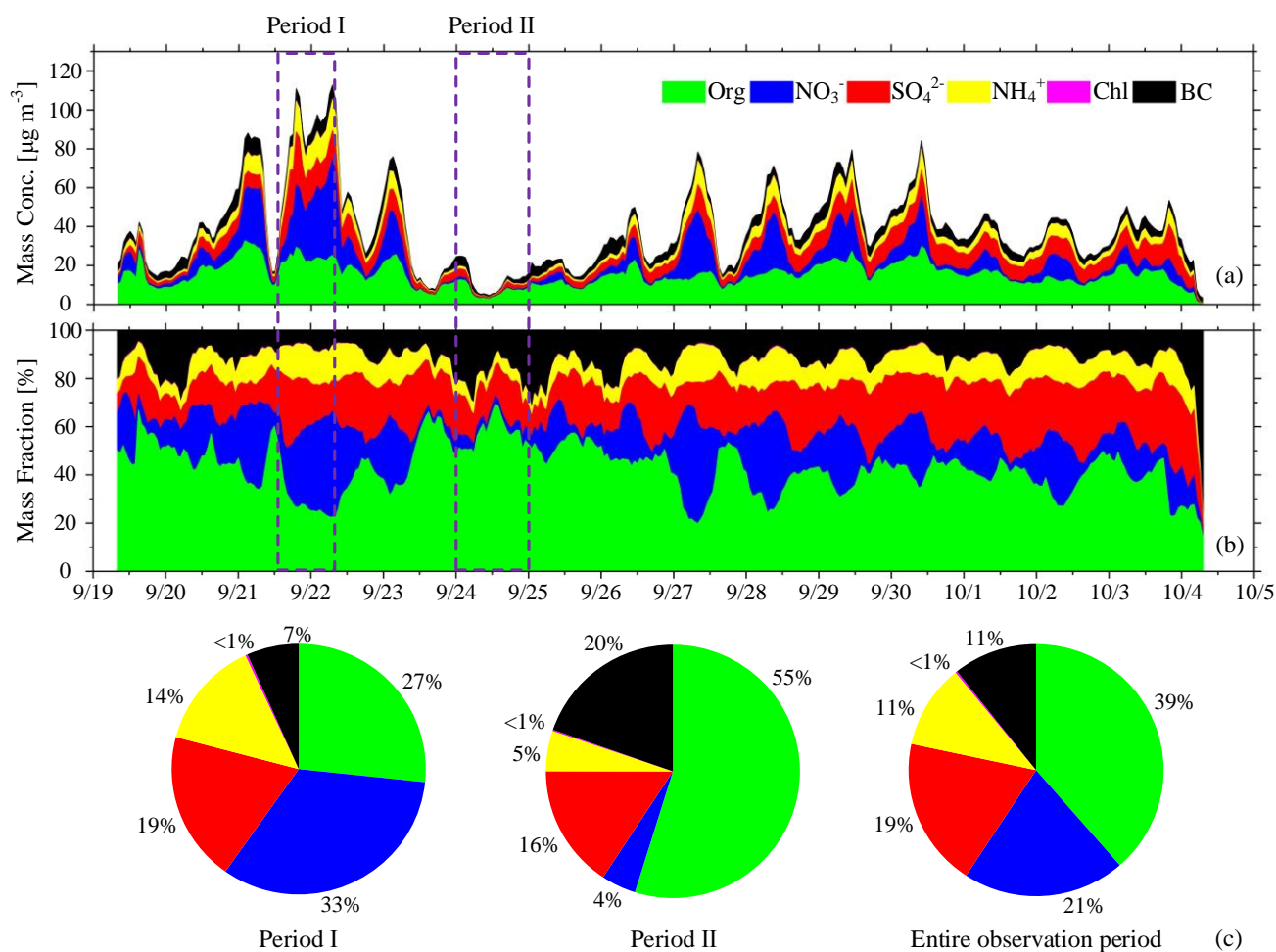
Figure 2: Hourly averaged time series (18 September to 4 October 2019) of the (a) scattering coefficient ($\sigma_{sp,525nm}$) measured by the dry nephelometer (unit: Mm^{-1}), (b) absorption coefficient ($\sigma_{ap,525nm}$; unit: Mm^{-1}), (c) single-scattering albedo ($\omega_{0(525nm)}$), (d) scattering Ångström exponent ($\alpha_{(450nm-635nm)}$), (e) hygroscopic enhancement factor at RH = 85% (f(RH = 85%, 525 nm)), and (f) mass concentration of PM$_{2.5}$ (unit: μg m^{-3}) measured at the Yizhuang station. The segments of the time series with a blue background represent the processes of deliquescence. The timescale is Beijing time (UTC + 8 h). The date in this figure is in the month/day format.
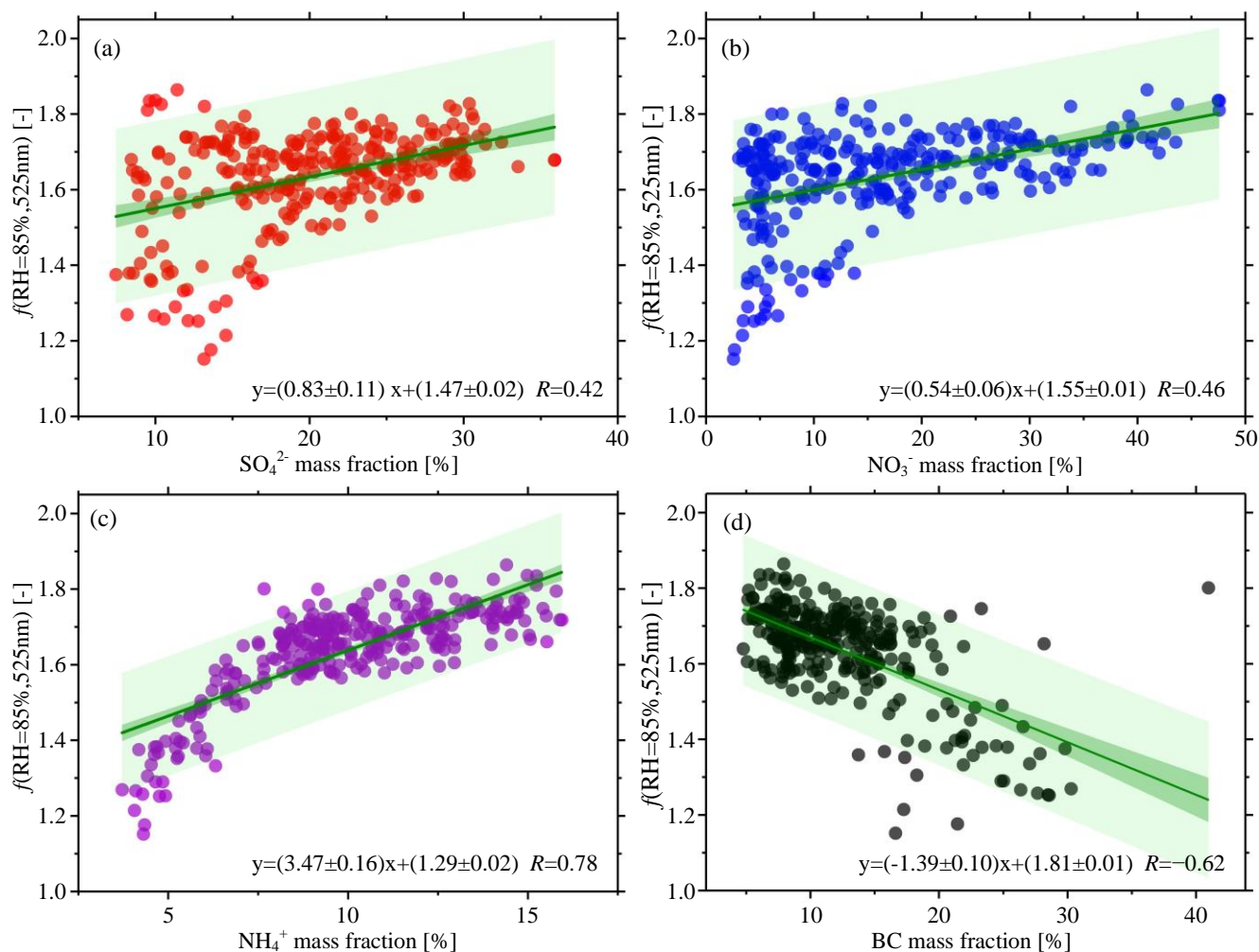
Figure 3: Wind dependence of (a) the single-scattering albedo $(\omega_{0(525nm)})$, (b) the scattering Ångström exponent $(\alpha_{(450nm-635nm)})$, (c) the hygroscopic enhancement factor at RH = 85% (f(RH = 85%, 525 nm)), (d) the mass fraction of BC, (e) the mass fraction of inorganic matter, and (f) the mass fraction of organic matter. The circular contours show the average change in wind speed and direction.

Figure 4: Time series of (a) mass concentrations (unit: μg m⁻³) and (b) mass fractions of NR-PM$_{2.5}$ species (unit: %) , i.e., organics, nitrate, sulfate, ammonium, and chloride. The timescale is Beijing time (UTC + 8 h). The date in this figure is in the month/day format. The pie charts in (c) show the average chemical composition of NR-PM$_{2.5}$ for Period I (the pie chart on the left), Period II (the pie chart on the middle) and the entire observation period (the pie chart on the right).

Figure 5: Hygroscopic enhancement factor f(RH = 85%, 525 nm) as a function of different aerosol chemical component mass fractions measured by the ACSM and the AE33: (a) sulfate (SO_4^{2-}) mass fraction, (b) nitrate (NO_3^-) mass fraction, (c) ammonium (NH_4^-) mass fraction, and (d) black carbon (BC) mass fraction. Solid green lines represent bivariate linear regressions. The darkgreen shaded areas denote 95% confidence levels, and the light-green shaded areas show the 95% prediction bands for the fits.
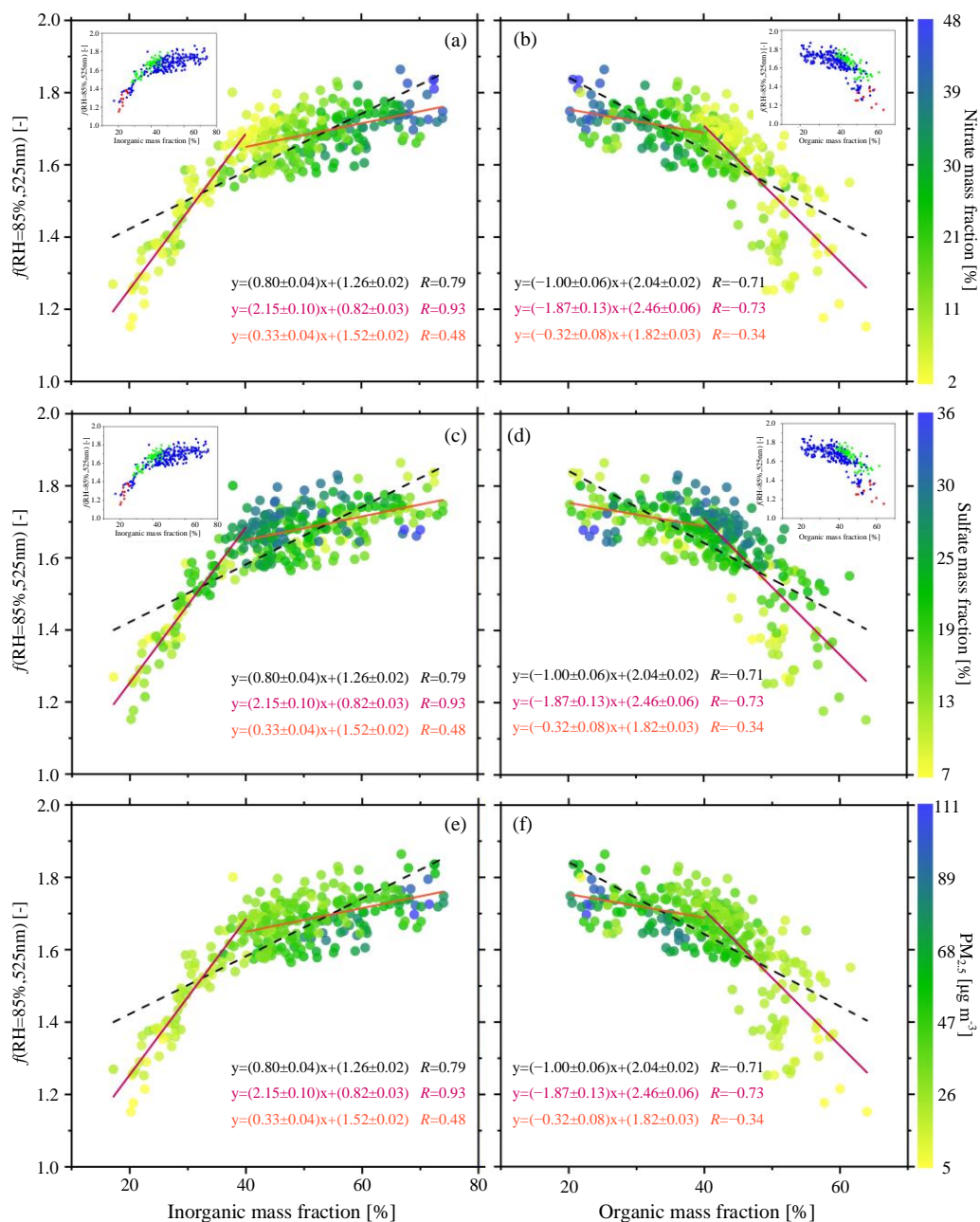
Atmospheric
Chemistry
and Physics
Discussions

Open Access
EGU

Figure 6: Hygroscopic enhancement factor $f(RH = 85\%, 525\ nm)$ as a function of organic matter mass fraction and inorganic matter mass fraction measured by the ACSM and the AE33: $f(RH = 85\%, 525\ nm)$ as a function of (a) inorganic matter mass fraction and (b) organic matter mass fraction colored by the nitrate mass fraction; $f(RH = 85\%, 525\ nm)$ as a function of (c) inorganic matter mass fraction and (d) organic matter mass fraction colored by the sulfate mass fraction; $f(RH = 85\%, 525\ nm)$ as a function of (e) inorganic matter mass fraction and (f) organic matter mass fraction colored by the mass concentration of $PM_{2.5}$. Dotted black lines denote bivariate linear regressions. The red and magenta lines are the best-fit linear regression lines through data points associated with mass fractions smaller than 40% and larger than 40%, respectively. The green dots in the inset figures represent deliquescence.
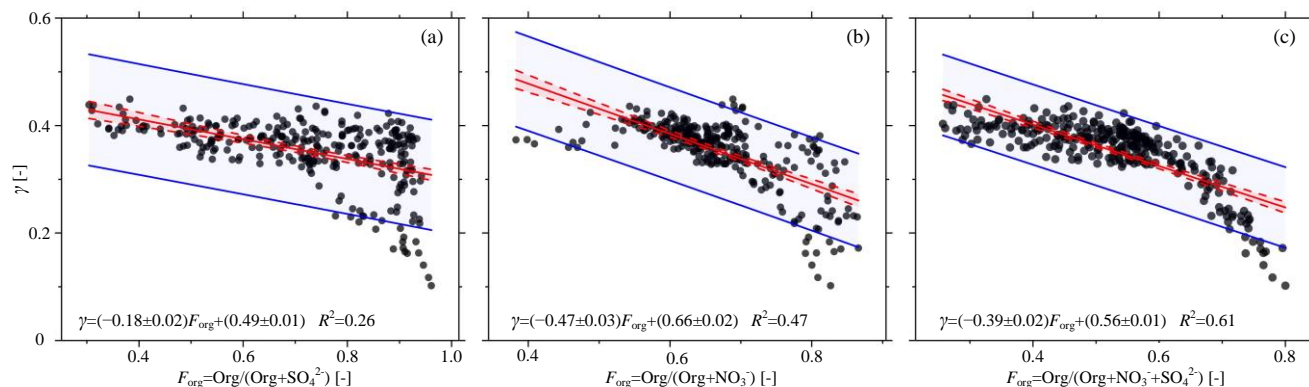
Figure 7: Scatter plots of γ as a function of the relative amounts of organic and inorganic matter (F_{org}): (a) F_{org}=Org/(Org+SO_4^{2-}), (b) F_{org}=Org/(Org+NO_3^-), and (c) F_{org}=Org/(Org+SO_4^{2-}+NO_3^-). Solid red lines show the linear fits, dotted red lines represent the 95%
610 **confidence levels, and solid blue lines represent the 95% prediction bands for the fit. The linear regression function and coefficient of determination (R^2) are given in each panel.**
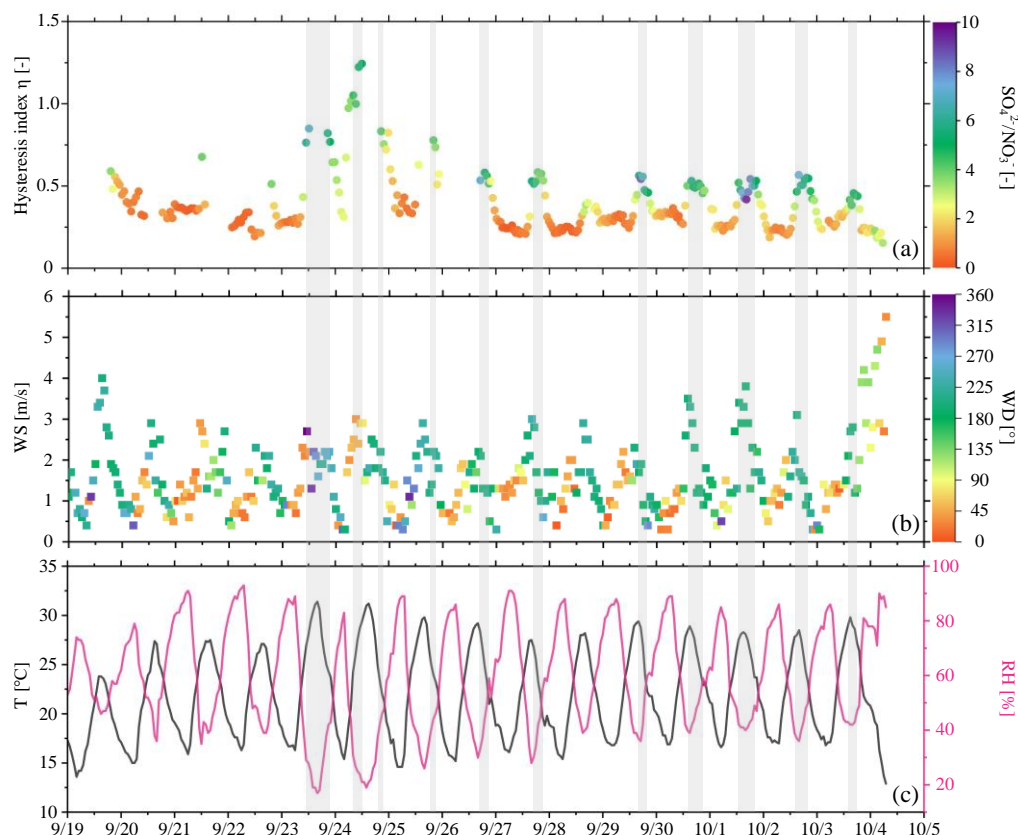

Figure 8: Time series of (a) hysteresis index η colored by the SO_4^{2-}/NO_3^- mass concentration ratio, (b) wind speed (WS) colored by wind direction (WD), and (c) ambient temperature (T) and relative humidity (RH). The segments of the time series with a grey
615 **background represent the processes of deliquescence. The date in this figure is in the month/day format.**
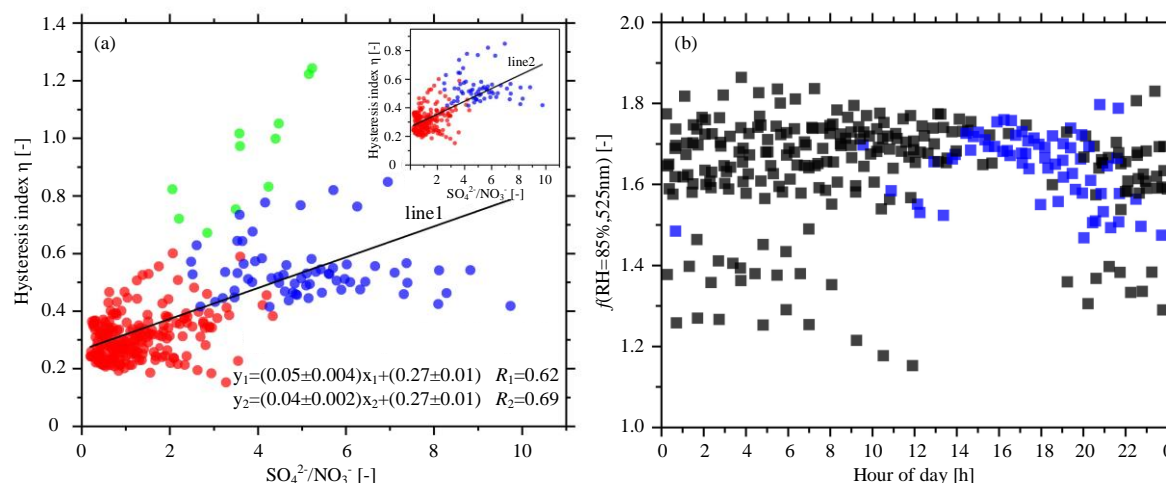
Figure 9: (a) Scatter plot of hysteresis index η as a function of the SO_4^{2-}/NO_3^- mass concentration ratio. Blue dots represent deliquescence, and red dots represent non-deliquescent processes. Green dots represent those data points with high systematic errors. The inset figure shows the scatter plot excluding the green dots. **(b)** Scatter plots of the observed f(RH = 85%, 525 nm) values for non-deliquescent (black) and deliquescent (blue) cycles.
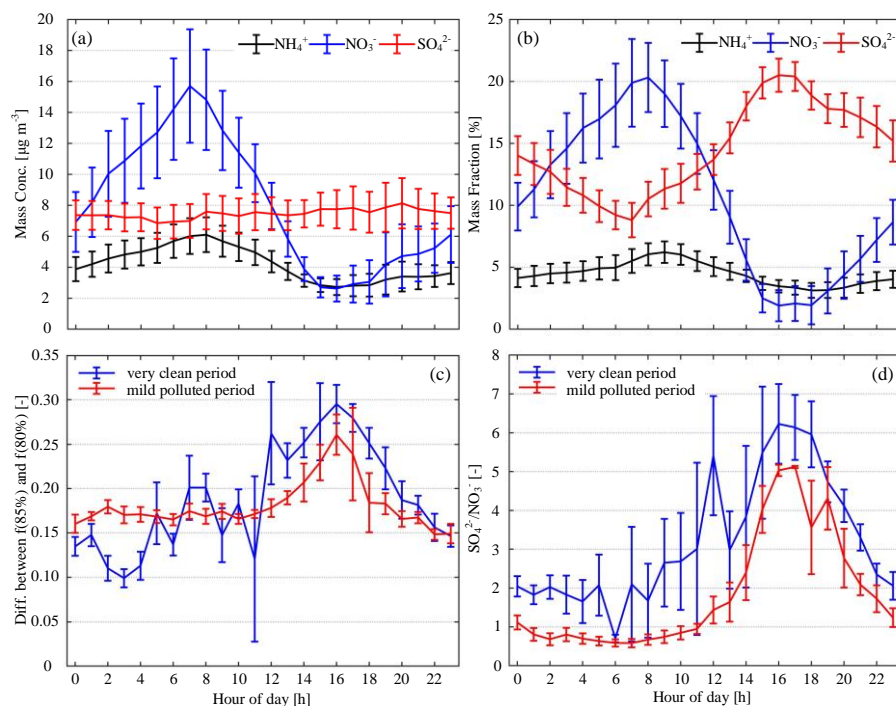

Figure 10: Average diurnal cycles of **(a)** mass concentration (unit: μg m^{-3}) and **(b)** mass fraction (unit: %) of ammonium (black curves), nitrate (blue curves), and sulfate (red curves) measured by the ACSM. **(c)** The difference between f(RH = 85%, 525 nm) and f(RH = 80%, 525 nm) and **(d)** the mass concentration ratio of sulfate to nitrate (SO_4^{2-}/NO_3^-) during the clean period (blue curve) and the moderately polluted period (red curve). Vertical lines are the standard deviations.
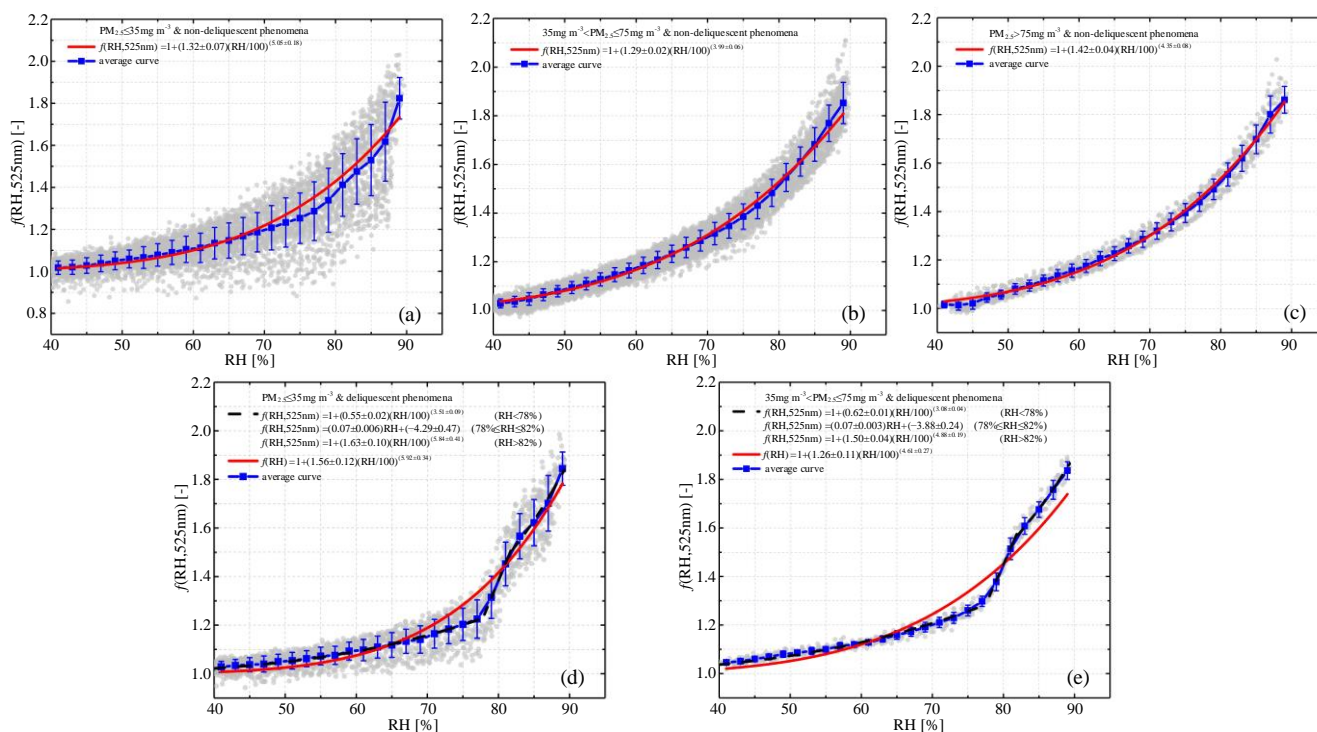
Figure 11: Fitted *f*(RH) of non-deliquescent curves (a-c) and deliquescent curves (d-e) for different pollution levels. Solid red lines represent fitted curves parameterized by Eq. (10). Black dotted lines represent the curves fit by segment function Eq. (12), and the solid blue lines represent the average curves.
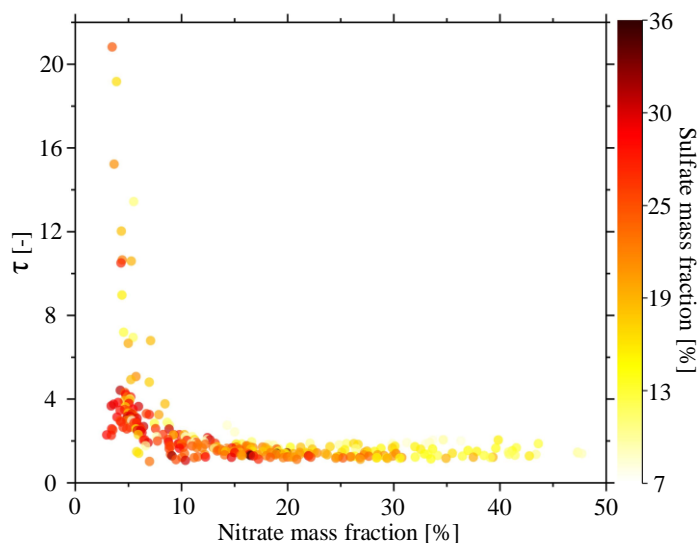

630

Figure 12: Scatter plot of the steepness index (τ) as a function of the nitrate mass fraction (unit: %), colored by the sulfate mass fraction (unit: %).

Table 1: Average $\sigma_{sp,525nm}$, $\sigma_{ap,525nm}$, $\omega_{0(525nm)}$, $\alpha_{(450nm-635nm)}$, f(RH = 85%, 525 nm), and PM$_{2.5}$ mass concentration values at different pollution levels.

	Entire observation period	PM$_{2.5}$ pollution levels [µg m^{-3}]		
		Very clean (PM$_{2.5}$ ⩽ 35)	Moderately polluted (35 < PM$_{2.5}$ ⩽ 75)	Heavily polluted (PM$_{2.5}$ > 75)
$\sigma_{sp,525nm}$ [Mm^{-1}]	266±179	106±52	290±94	546±86
$\sigma_{ap,525nm}$ [Mm^{-1}]	51±24	41±22	53±20	68±20
$\omega_{0(525nm)}$ [-]	0.80±0.09	0.73±0.08,	0.84±0.04	0.89±0.02
$\alpha_{(450nm-635nm)}$ [-]	1.48±0.17	1.55±0.19	1.46±0.14	1.27±0.14
f(RH=85%,525 nm) [-]	1.64±0.13	1.49±0.16	1.70±0.06	1.71±0.05
PM$_{2.5}$ [µg m^{-3}]	44±25	22±9	51±12	90±9

635

Table 2: Curve-fitting parameters of f(RH) at 525 nm for different aerosol types using Eq. (10).

Classification			m	n	a	b	Reference
Non-deliquescence	Very clean		1.32±0.07	5.05±0.18			
	Moderately polluted		1.29±0.02	3.99±0.06			
	Polluted		1.42±0.04	4.35±0.08			
Deliquescence	Very clean	RH < 78%	0.55±0.02	3.51±0.09			This study
		RH > 82%	1.63±0.10	5.84±0.41			
		78%<RH<82%			0.07±0.006	−4.29±0.47	
		40%<RH<90%	1.92±0.41	6.96±1.63			
	Moderately polluted	RH < 78%	0.62±0.01	3.08±0.04			
		RH > 82%	1.50±0.04	4.88±0.19			
		78%<RH<82%			0.07±0.003	−3.88±0.24	
		40%<RH<90%	1.63	5.61			
Clean			1.20±0.06	6.70±0.27			Pan et al. (2009)
Polluted			2.30±0.03	6.27±0.10			
Dust			0.64±0.04	5.17±0.4			
Locally polluted			1.24±0.29	5.46±1.90			Zhang et al. (2015)
Northerly polluted			1.20±0.21	3.90±1.27			
Dust-influenced			1.02±0.19	4.51±0.80			